Fuel 197 (2017) 310–319

Contents lists available at ScienceDirect

Fuel

journal homepage: www.elsevier.com/locate/fuel

Full Length Article

Evolution of pore structure in gas shale related to structural deformation

Mingliang Liang, Zongxiu Wang *, Li Gao, Chunlin Li, Huijun Li

Institute of Geomechanics, Key Lab of Shale Oil and Gas Geological Survey, Chinese Academy of Geological Sciences, Beijing 100081, China

HIGHLIGHTS

- Pore character in shale samples from the detachment deformation belt was studied.
- Diagenesis and shale composition controls on pore structure and adsorption capacity.
- The structural deformation affected the evolution of pore size distribution in shale.
- Evolution of macroporosity between deformed and undeformed samples is different.
- The deformed shale has a higher percentage of macropores and lower of mesopores.

ARTICLE INFO

Article history:
Received 14 December 2016
Received in revised form 8 February 2017
Accepted 14 February 2017

Keywords:
Tectonic deformed shale
Pore volume
Porosity
Surface area
Pore size distribution
Pore structure evolution

ABSTRACT

The pore characterization in shale depends on the shale composition, affected by the tectonic deformation. To obtain information about the influence of tectonic deformation on shale pore characteristics, the geochemical, mineralogical, structural and textural properties analysis, porosity and pore structure feature investigations are performed using two sets of shale (deformed shale and undeformed shale) collected from the same shale bed of the Wufeng-Longmaxi Formations (Upper Ordovician-Lower Silurian) of southeast of Sichuan Basin, China. The diagenetic environment and shale composition controls on total porosity and pore structure. Both undeformed and deformed samples have a similar porosity (>1.3%). All-scale pore structure analysis reveals that the pore size distribution of all shale samples is mainly from 0.35 nm to 1.E+5 nm. The surface area of both undeformed and deformed samples were mainly contribution from the micropores (>82%). The geochemical and mineralogical analysis suggested that there was a good correlation between the organic maturity, quartz content and shale deformation. Tectonic stress and structural deformation have an effect on the pore surface area and adsorption capacity of shale. Undeformed shale has a higher surface area and nitrogen adsorption capacity, and the strong deformed shale samples have the lowest surface area and nitrogen adsorption capacity. The total porosity was positively correlated with the micro- and mesopores pore volume for undeformed shale ($R^2 > 0.85$), while the porosity of deformed shale was only related to the macropores pore volume ($R^2 = 0.77$). Experimental analysis showed that all shale samples from the same bed had similar total porosity and pore volume, while the deformed shale had notable higher macropores percentages than undeformed shale. The results indicated that accompanied by tectonic deformation, the porosity, total pore volume and micropores content did not change significantly, while the percentages of pores were changed as macropores increased and mesopores decreased. The proportions of micro-, meso- and macropores were changed by structural deformation. Part of mesopores was disappeared due to compression of the tectonic stress, and macropores were generated due to the development of microcracks.

1. Introduction

The global shale gas "Revolution" from North America to China expanded the views on shale with that transformed the role of shale from conventional source rocks and cap rocks into unconventional reservoirs [1–6]. Compared to conventional reservoirs, shale was a tight reservoir characterized by abundant nano-pores [1,7–9].The knowledge of the pore structure properties, including pore size distribution (PSD), surface area (SA), pore volume (PV) and porosity parameters were essential to determine the shale reservoir characters. According to the classification of International Union of Pure and Applied Chemistry (IUPAC) [10,11], pores are divided into micropores (pore width <2 nm), mesopores (pore

* Corresponding author.
E-mail address: wangzongxiu@sohu.com (Z. Wang).

http://dx.doi.org/10.1016/j.fuel.2017.02.035
0016-2361/

width between 2 and 50 nm) and macropores (pore width >50 nm). Nuclear magnetic resonance (NMR), small-angle and ultra small angle neutron scattering (SANS/USANS), nano-computed tomography (Nano-CT) and other radiation methods be used to conduct non-destructive analysis and acquire detailed data rapidly [1,12,13]. Image analysis methods can be used to observe the geometry and pore size in shale through transmission/scanning electron microscopy (TEM/SEM) and other high resolution microscopes. Moreover, Researchers often conduct quantitative analyses with the fluid invasion method such as mercury injection capillary pressure (MICP) and low-pressure gas (LPG) adsorption (carbon dioxide and nitrogen) to determine the shale pore size distribution and use theoretical models to calculate the specific surface area, the volume and other parameters [1,14–17].

Scholars have already conducted studies on pore structure properties of shale in different strata and various regions [2–6] by measurement techniques mentioned above. It has been found that the formation and evolution of pore structure in shale affected by various geological conditions include the geochemical and thermal maturity [18–20], lithology and diagenesis [6,14–17]. For example, Ross and Bustin [14] studied the effects of various shale attributes (organic/inorganic composition, thermal maturity) upon pore structure by quantitative analyses with the fluid invasion method. The results of low pressure nitrogen (N_2) and carbon dioxide (CO_2) adsorption suggested that the thermally mature shale with 1.6–2.5% vitrinite reflectance values (VRo) have higher micropore volumes and surface area than shale have lower thermal maturity ranging from 0.9 to 1.3%VRo. While mercury injection capillary pressure (MICP) observations showed that in diameter range of 3–360,000 nm, clay-rich samples have unimodal mesopores that pore diameters of 7–8 nm, in contrast to quartz-rich shales which show a dominance of macropores. Scattered electron microscopy (SEM) and mercury injection capillary pressure (MICP) were used by Chalmers et al. [4,15–17] to study the pore characteristics of North America with different total organic carbon (TOC) contents and mineral composition. The results showed that the samples contain higher quartz, moderate clay and high TOC content have more balanced ratios between micro-, meso- and macroporosity and high permeability.

In recent years, the dynamic evolution of pore structure has attracted more attention [18–20]. Sun et al. [20] analyzed the formation and development of the nanoporosity in continental shale before and after hydrous pyrolysis experiment by N_2 adsorption to measure the pore structure of shale in different thermally mature stage. The results showed that the nano pore volume and the N_2 Brunauer-Emmett-Teller (BET) specific surface area were positively correlated with the pyrolysis, with increasing temperature, the pore volume and N_2 BET specific surface area of the micropores, mesopores and macropores all increased. Chen and Xiao [19] used N_2 and CO_2 adsorption to measure the pore structure of artificially matured samples with vitrinite reflectance values (VRo) ranging from 0.69% to 4.19%, finding that the microporosity and mesoporosity increases with thermal maturity after the oil window stage, and suggested those increases were attributed to the formation of porosity within organic matter and/or mineral–organic matter groundmass, rather than in the pure clay minerals, and they subdivided the evolution of nanopores into three stages: formation stage (VRo from 0.6% to 2.0%), development stage (VRo from 2.0% to 3.5%) and conversion and destruction stage (VRo > 3.5%). Focused ion beam milling combined with scanning electron microscopy (FIB–SEM) techniques were used by Curtis et al. [18] to analyzing organic porosity in Woodford shale samples with different VRo (from 0.51% to 6.36%). The result indicated that thermal maturity alone was not enough to predict porosity in organic matter (OM), but other factors like OM composition were also needed to be considered.

Although the formation and evolution of pore structure in shale have been described in previous works, the genesis and evolution of pores in shale during geological and tectonic process remain poorly understood. This may be caused by the different geological factors, such as mineral composition, TOC, OM type and chemical composition, diagenesis and maturity [14–20], all controlled by geological and tectonic process. With the success of shale gas exploit in South China, effect of tectonic process on reservoir characters has recently attracted more attention [5,21–24]. Compared to North America, the geological conditions of gas shale reservoirs in South China are highly diversified and complicated due to the multi-tectonic movement, which transformed the structure of shale seams and resulted in structure deformed shale with unique reservoir properties [21–24]. For example, as the first commercial shale gas field outside the North America, one of the most important controlling geological factors in the Fuling shale gas field in southeastern margin of the Sichuan Basin was strong structural deformation of shale [5,21–22]. It is necessary to study how pore structure develops in gas shale influenced by tectonic deformation. Ma et al. [23] investigated the pore structure of the mylonitized shale sample by FESEM and N_2 adsorption analysis, and found that the mylonitized shale has high specific surface area and high methane adsorption capacity. Ibanez and Kronenberg [25] have explained the deformational and microstructural changes under variable confinement for illite rich shale. Shale gas and coalbed methane (CBM) reservoirs are in formally grouped as unconventional because gas is trapped in part by sorption processes [14]. Several previous workers have focused on the pore characteristics and adsorption gas characteristics of tectonically deformed coals [26–27], which provide references to the study on deformed shale. Although previous studies have provided useful insight to evolution of pore structure in shale during thermal maturity and in CBM related to deformation structures, the prediction of structural deformation change in pore structure of shale in geological condition still remains quite challenging.

In the present study, pore structure feature investigations are performed using two sets of shale samples (deformed shale and undeformed shale) collected from the same shale bed of the Wufeng-Longmaxi Formations (Upper Ordovician-Lower Silurian) of southeast Sichuan Basin, China. The relationship between geological conditions include geochemical, mineralogical and structure properties was investigated. The influence of structural deformation on pore structure was studied. The influence of shale composition and different degrees of deformation on pore structure was also discussed. These results provide evidence to the evolution of pore structures of shale affected by tectonically deformation.

2. Samples and experiments

2.1. Sample selection

To avoid influences from other factors during the investigation of the influence of the tectonic deformation structures on pore structure, all experimental outcrop samples were selected from the same area and stratum (Wufeng-Longmaxi formations, Yongshun, China). Except for erosion thickness and current buried depth, the other geological conditions of the shale samples include stratigraphic, geochemical, petrological and especially the tectonic deformation property are similar to the Fuling gas field [21,22,24,28]. Samples sitting at southeastern Sichuan Basin, China and the detachment structural deformation control across the Wufeng-Longmaxi formations shale in this area [24,28]. As the

main detachment structure belt [24], the Wufeng-Longmaxi formations shale layer developed multi-layer subdivided slip structural deformation. The detachment fault mirrors (FMs), scratches and micro-fold deformation phenomena were commonly present in Wufeng-Longmaxi shale outcrops. A suite of samples were subset to two sets of deformed shale and undeformed shale for this study due to their variability of texture, fabric and structure properties (Figs. 1 and 2). The features of the experimental samples are shown in Table 1. The sample number was abbreviated as U1, U2, U3 (Undeformed shale) and D1, D2, D3, D4, D5 (Deformed shale), the deformed samples subsets to strong deformed shale (D1, D2, D3) and weak deformed shale (D4, D5). The samples of U3 were collected from the thick sandy shale, and the other samples were collected from the thin siliceous shale. The stratigraphic relationships of the samples are show in Fig. 1.

2.2. Experimental and methods

To evaluate the influence of tectonically deformation on shale reservoir characteristics by comparing the deformed shale and undeformed sample subsets, 14 shale samples (9 undeformed samples from 3 beds) were collected from this Yongshun outcrop (Fig. 1). However, not all the 14 samples were examined. Among these samples, all samples were analyzed to determine the organic geochemistry and mineralogy, the undeformed samples taken from same bed have similar composition characteristics, 8 samples (3 undeformed samples and 5 deformed samples) were selected for mercury injection capillary pressure (MICP) and low-pressure gas (LPG) adsorption to determine the pore structure including the porosity, pore-size distribution (PSD), surface area (SA) and pore volume (PV).

2.2.1. Geochemical and mineralogical

Before geochemical and mineralogical analyses, samples crushed to 180-200mesh. The TOC content was collected using a Leco C/S-344 Carbon/Sulfur analyzer. The stable carbon isotope was determined using a Finnigan MAT 252 mass spectrometer. A 3Y-Leica DMR XP microscopy equipped with a microphotometer was used to measure the vitrinite reflectance values (VRo) of samples. Each sample was determined by 30 measurements on vitrinite particles at least. The crushed samples were mixed with ethanol, hand ground in a mortar and pestle and then smear mounted on glass slides for X-ray diffraction (XRD) analysis using a D/Max-III analyzer at 40 kV and 30 mA. The relative mineral contents were estimated semi-quantified using the area under the curve for the major peaks.

2.2.2. Porosity, pore size distribution (PSD), pore volume (PV) and surface area (SA)

To fully evaluate the pore size distribution and porosity, samples were crushed (2–5 mm) and dried at 110 °C, and then preformed both mercury porosimetry and low pressure gas adsorption analyses.

The mercury injection capillary pressure (MICP) analysis using a Poremaster GT60, and intruded with mercury from 1.5 to 60,000 Psi, the measured pressure range equates to the pore diameter range of 0.003–1000 μm (7–120,000 nm in this study). The pore size distributions of mesopores and macropores were determined using the Washburn equation [29]. The minimal pore diameter limit of 7 nm is within the mesopore range, and mercury porosimetry cannot detect micropores within the pore structure. Porosity is determined by mercury immersion (bulk density) coupled with helium pycnometry (skeletal density).

Low pressure gas adsorption analyses have been used to measure the PSD both micropores and mesopores using both nitrogen adsorption at −196 °C and carbon dioxide adsorption at 0 °C by a Micromeritics ASAP 2020 HD88 analyzer. The PSD, PV and SA analysis of combined the N_2 and CO_2 gas adsorption by the same calculation models of density function theory (DFT) [1,11,30–31]. The development of DFT models has led to a better understanding of adsorption processes in well ordered systems compared to the more conventional models [32], used in the present study to analyzed N_2 and CO_2 gas adsorption data.

The pore characteristics including SA, PV and PSD will different between the two techniques (MICP and gas adsorption analyses) because of sample preparation, analytical models and calculation models, analysis method of combined the mercury intrusion and gas adsorption only used to determine the relative content

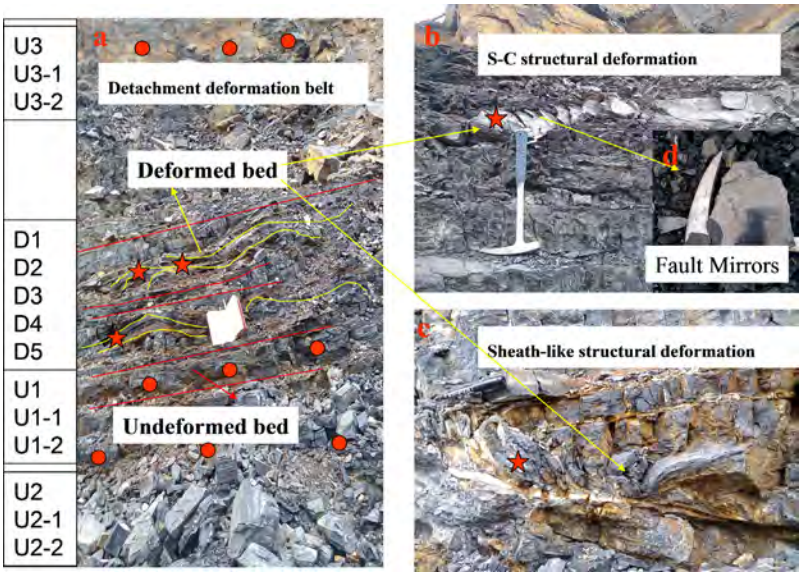

Fig. 1. Location of study area is in southeastern Sichuan Basin, Yongshun, China. And the detachment structural deformation control across the Wufeng-Longmaxi formations shale in this area. (a): The stratigraphic relationships and structural deformation characteristics of the samples, (b): S-C structural deformation shale, (c): Sheath-like structural deformation shale (d): Fault mirrors (FMs) of the deformed shale. ★: Deformed shale samples, ●: Undeformed shale samples. The height of the notebook is 20 cm (a), length of the hammer is 38 cm (b), and the length of the pen is 14 cm (c). See Fig. 2 and Table 1 for texture and structure properties of these deformed samples.

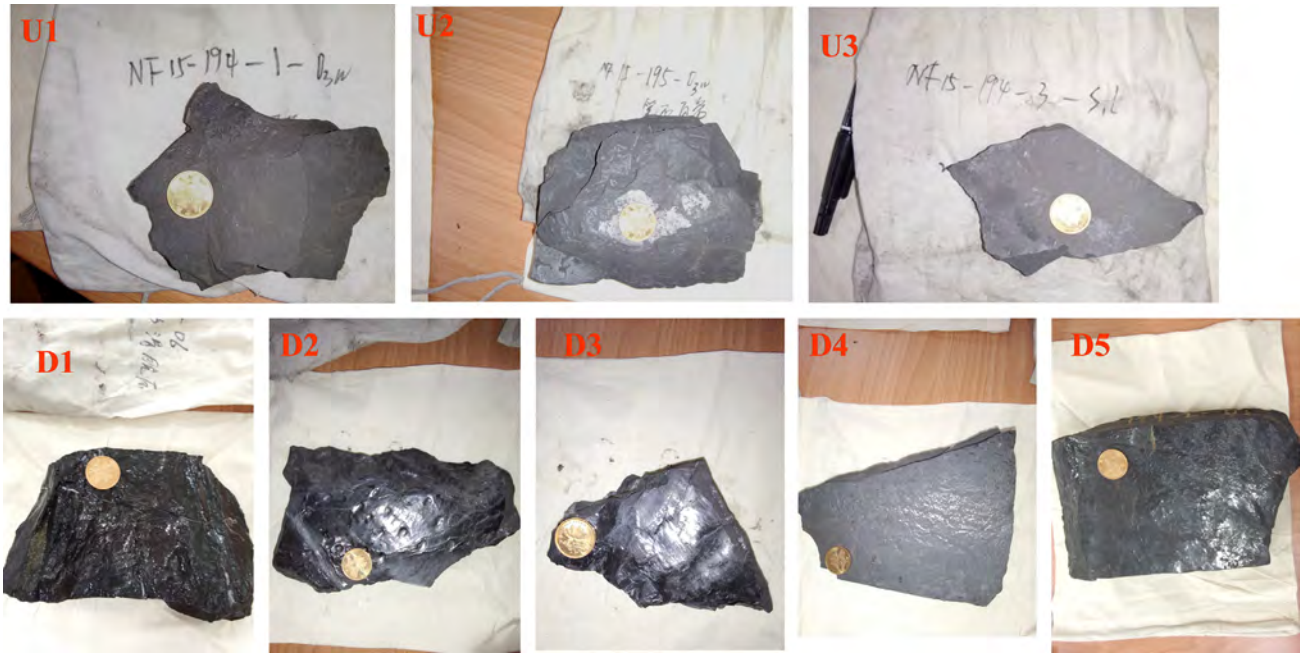

Fig. 2. Undeformed shale and deformed shale samples, the sample ID was abbreviated as U1, U2, U3 (Undeformed shale) and D1, D2, D3, D4, D5 (Deformed shale). The undeformed shales have original parallel bedding, and the primary structure of shale can be observed. The detachment fault mirrors (FMs) can be observed on the deformed shales. And the deformed samples were subset to two sets of strong deformed shale and weak deformed shale due to their difference on the degree of deformation strength. The D1, D2, and D3 were strong deformed shales that the primary structure was damaged and the parallel bedding has almost disappeared due to deformation, and the fractures and mineral filling development in the strong deformed shales. The D4 and D5 were weak deformed shales that have original parallel bedding, and FMs developed in the surface of fault. The Coin diameter is 20.5 mm.

Table 1
The features of the experimental samples.

Sample ID	TOC (%)	VRo (%)	δC_{13} ‰(PDB)	Quartz (%)	Carbonate (%)	Clay (%)	Texture and fabric features of macroscopic hand specimens
U1	3.9	2.57	−30.4	41	nd	44	Undeformed shales. Shale primary structure can be observed. Shale has original parallel bedding.
U2	2.5	2.78	−30.8	40	2	41	
U3	2.0	2.77	−30.9	34	11	33	
U-mean (9)	2.8	2.76	−30.7(3)	42	4.6	38	
D1	2.1	3.01	−30.6	77	nd	14	Strong deformed shales. The primary structure of shale is damaged and the parallel bedding has almost disappeared due to deformation. Fractures and mineral filling development. The plastic deformation of shale is obvious. Shale shows cleavage structure and cleavage surface is smooth with fine-grained powder coatings.
D2	6.6	2.86	−31.0	64	nd	26	
D3	1.0	2.91	−31.3	77	nd	16	
D4	1.8	2.90	−30.6	46	nd	41	Weak deformed shales. Shale has original parallel bedding. Shale shows cleavage structure and cleavage surface is smooth with fine-grained powder coatings.
D5	3.0	3.00	−31.1	71	nd	20	
D-mean (5)	2.9	2.93	−30.9	67	nd	23	

TOC – total organic carbon (%); VRo – vitrinite reflectance values (%); (Number): number of measured samples.

Table 2
Pore volume characteristics of the samples.

Sample ID	Gas absorption		MICP			Relative content* (%)		
	Micropore (μL/g)	Mesopore (μL/g)	Mesopore (μL/g)	Macropore (μL/g)	Porosity (%)	Micropore (%)	Mesopore (%)	Macropore (%)
U1	6.4	4.8	186.7	231.9	2.0	37.6	27.9	34.6
U2	5.7	8.4	175.5	122.9	1.6	28.5	42.0	29.4
U3	10.4	20.9	2198.4	330.0	7.5	30.3	60.6	9.1
D1	4.5	2.2	73.9	185.7	1.3	36.6	18.1	45.4
D2	5.3	6.7	73.8	143.3	1.6	21.2	26.8	52.0
D3	2.2	0.4	14.2	273.2	3.8	22.6	3.8	73.5
D4	4.5	3.8	148.7	172.1	2.5	28.5	23.8	47.7
D5	5.2	4.4	214.3	387.4	4.5	15.1	12.9	71.9

* The relative contents of different pore size distributions with PV were calculated by set the mesopore PV as referenced value.

Table 3
Pore surface area characteristics of the samples.

Sample ID	Total SA of Gas absorption by different model				Gas absorption (DFT)		MICP		Relative content*(%)		
	CO_2 (DR) (m^2/g)	CO_2(DFT) (m^2/g)	N_2(BET) (m^2/g)	N_2(DFT) (m^2/g)	Micropore (m^2/g)	Mesopore (m^2/g)	Mesopore (m^2/g)	Macropore (m^2/g)	Micropore (%)	Mesopore (%)	Macropore (%)
U1	17.53	9.87	23.52	30.79	15.46	1.68	1.72	0.01	90.2	9.8	0.0
U2	13.36	7.35	21.66	29.17	13.01	1.86	1.46	0.03	87.3	12.5	0.3
U3	29.98	20.05	39.55	52.28	27.10	5.68	10.38	0.49	82.0	17.2	0.8
D1	13.44	8.21	10.73	15.06	11.63	0.92	0.72	0.03	92.5	7.3	0.3
D2	12.19	5.94	12.46	18.98	11.42	1.04	0.58	0.00	91.7	8.3	0.0
D3	6.94	2.90	4.61	7.95	6.15	0.09	0.05	0.00	98.4	1.5	0.1
D4	10.72	5.72	16.01	21.92	10.20	1.43	0.78	0.00	87.7	12.3	0.0
D5	13.11	6.77	18.38	25.26	11.74	1.91	0.55	0.00	85.9	14.0	0.1

* The relative contents of different pore size distributions with SA were calculated by set the mesopore SA (DFT) as referenced value.

percentage of micro-, meso- and macropores in this article by set the mesopores as a referenced values (Tables 2 and 3).

3. Results and discussion

3.1. Shale composition

The organic geochemistry and mineralogy data of the samples are shown in Table 1. The characteristics of shale composition (organic matter and mineralogical composition) are believed to be some of important properties controlling pore structure and gas storage capacity in shales [14–17]. The organic richness and mature stage have resulted in the production of large amounts of gas in key productive areas of the Barnett Shale [33]. Both deformed and undeformed shale samples display high-quality organic matter richness features (TOC > 1%) and within the gas generation window (VRo values of 2.57%–3.01%), suggested that the shale samples have high-quality organic matter richness for shale gas generation over geological time. The VRo for structure deformed shales (2.86% and 3.01%) slightly higher than undeformed samples (2.57% and 2.78%), indicating that tectonic deformation and stress have a certain influence on the maturation evolution of organic matter [27,34]. Both deformed and undeformed shales have similar carbon isotope values of -30.4‰ to -31.3‰. The carbon isotopic compositions allow good insights to the provenance of the organic matter, the isotope analysis often used for paleoenvironmental reconstructions [35–36]. Based on the range of carbon isotope values, we assume that the organic matter in the Wufeng-Longmaxi shales is 100% marine organic matter [35–37]. The comparison of evolutionary changes in the deformed shale and undeformed shale with respect to the organic geochemistry suggests that the structural deformation almost have no effect on organic matter in shale, except for the slight increase in maturity.

Except for U3 of sandy shale, all other samples were dominated by quartz and clay (Table 1), and the sums add up more than 80%, were classified as biogenic siliceous shale, due to the high quartz contents above 40% with high TOC content above 2.0%. The evidence for graptolite and radiolarians provides high levels of biogenic siliceous and organic carbon to the Wufeng-Longmaxi Shales [38]. Note that the deformed shales contain higher amounts of quartz but relatively lower amounts of clay than the undeformed shales. In general, since different minerals have different physical properties, the shale with high quartz will have low Poisson's ratio, high Young's modulus, high shear modulus and high brittleness [39–40]. As a result, the shale with high quartz was conducive to produce fractures under tectonic stress. The parts of extra quartz content in fracture filling of deformed shales may come from the hydrothermal source, after the tectonic deformation and fracture generations.

3.2. Low pressure gas adsorption

Low pressure nitrogen isotherms for deformed and undeformed shale samples showed in Fig. 3. The nitrogen adsorption-desorption curve of shale can be used to analyze the pore structure characteristics [1,11,19–20]. Because capillary condensation and capillary evaporation often do not occur at the same pressure, there is a detached portion between the corresponding desorption and adsorption isotherm branch. The hysteresis loop was observed for all samples, and the desorption branch always above the adsorption branch. The adsorption-desorption curves show an inverse "S" shape, according to the classification of gas adsorption isotherms made by IUPAC [10,11], type IV isotherms and H3 hysteresis loops correspond to the experimental samples. Isotherms with Type H3 hysteresis loops are usually materials comprised of aggregates of plate-like particles forming slit-like pores, which are consistent with the characteristics of parallel layered shales rich in layered clay minerals. Within the gas generation window (VRo > 2.60%), the sample LCG (TOC = 29.1%) always has a larger detachment than sample DL (TOC = 8.63%) and EP((TOC = 0.18%) [19]. A larger detached portion observed between the desorption and adsorption isotherm branch in deformed sample 2, may be interpreted as organic matter pores has a strong adsorption capacity and the sample D2 has the highest TOC content (6.6%). When the relative pressure P/P0 close to 1, the nitrogen adsorption quantities of undeformed samples are about 10–30 mL/g, while the weak deformed samples are about 8 mL/g and strong deformed samples are about 2–5 mL/g, respectively. No dramatic changes of adsorption capacity in tectonic deformation coals were observed by Pan et al. [26]. With the uniaxial compression simulation experiment, Zhang, et al. simulates the process of weak brittle deformation of shale at room temperature, and the methane adsorption capacity of shale after simulation was always about 10% lower than that of the original shale, far less than the difference value caused by TOC and thermal maturity differences [41]. The undeformed sample U3 far away from the deformation bed contains higher carbonate mineral contents have the highest nitrogen adsorption quantities. And the strong deformed samples D1, D2 and D3 have the lowest nitrogen adsorption quantities. The adsorption capacity is mainly related to the surface area, while the surface area is mainly provided by the nano-pores (micro- and mesopore fractions).

Low pressure gas adsorption analyses have been used to measure the PSD both micropores and mesopores. The development of density function theory (DFT) models has led to a better understanding of adsorption processes in well ordered systems compared to the more conventional models[11,32]. The DFT calculation model to provide a more reliable approach to pore size analysis over the complete nanopore range containing micropores and mesopores [30–31]. The PSD, PV and SA were derived by analysis of the combined the N_2 and CO_2 gas adsorption data by the

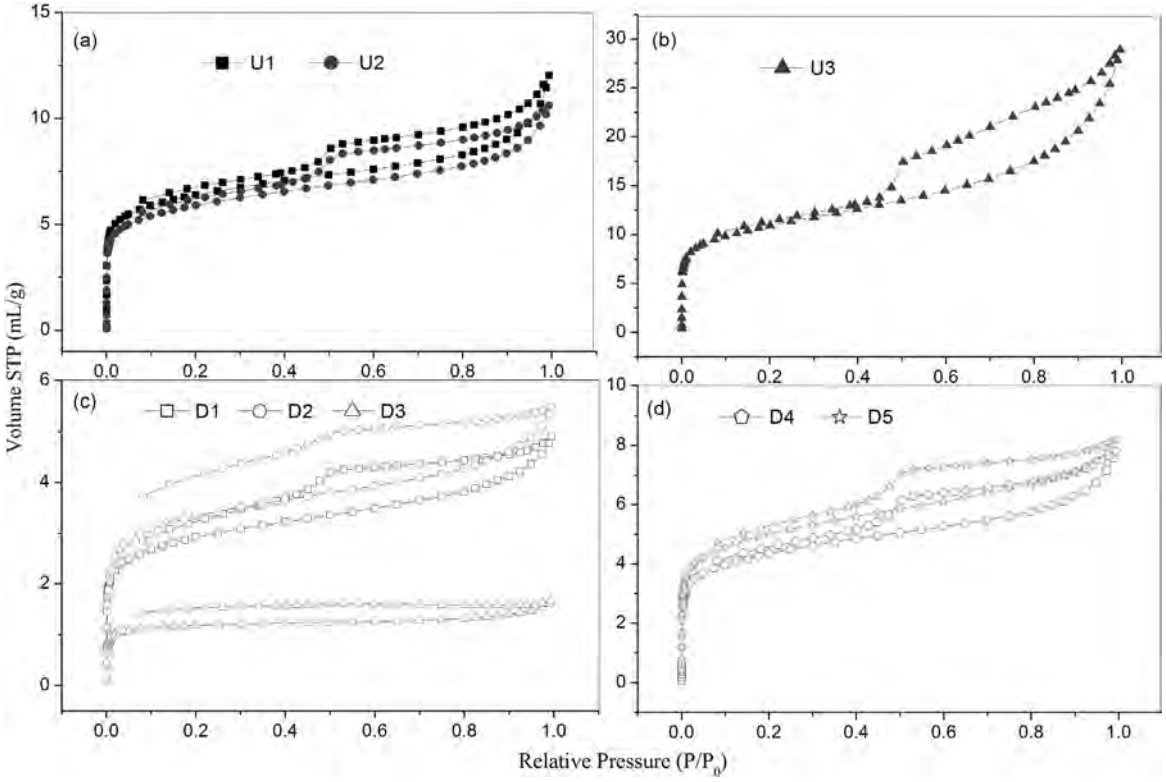

Fig. 3. Nitrogen isotherms for undeformed samples (a) and (b), strong deformed samples (c) and weak deformed samples (d).

same calculation models of density function theory (DFT). The two gas adsorption methods were combined through incremental PV and SA plots (Figs. 4 and 5). According to Figs. 4 and 5, the incremental curves from the DFT model versus pore diameter results perfectly reflect PSD. The Dubinin-Radushkevich (DR) and Brunauer-Emmett-Teller (BET) models can used to calculate the total SA using CO_2 and N_2 adsorption data, respectively. The Table 3 showed the surface area (SA) calculated by different models. Both deformed samples and undeformed samples show a significant part of the pore volume between the diameters of 0.3 and 2 nm (micropore size fraction) that contributes to most of the surface area measured by gas adsorption analysis. The undeformed sample U3 contains the largest micro- and mesopore PV and the deformed sample D3 contains the least. Note that there was a significant volumes of pores with a diameter between 2 and 50 nm (mesopores fraction; Fig. 4a) in sample U3, suggested that the diagenetic environment and carbonate solution pores might controlled the development of mesopores in this sandy shale sample. The deformed sample D3 contains the least micropore and mesopore PV, interpreted as the lowest TOC contents (1.0%) and low clay mineral contents (16%). Excluding the sample U3 with significantly different mineral compositions, there were no dramatic changes of micropore PV and SA in deformed shale samples were observed. The tectonic deformation has little effect on the micropores, and the formation and evolution of micropores mainly related to the organic matter. It was believed that the SA and adsorption capacity

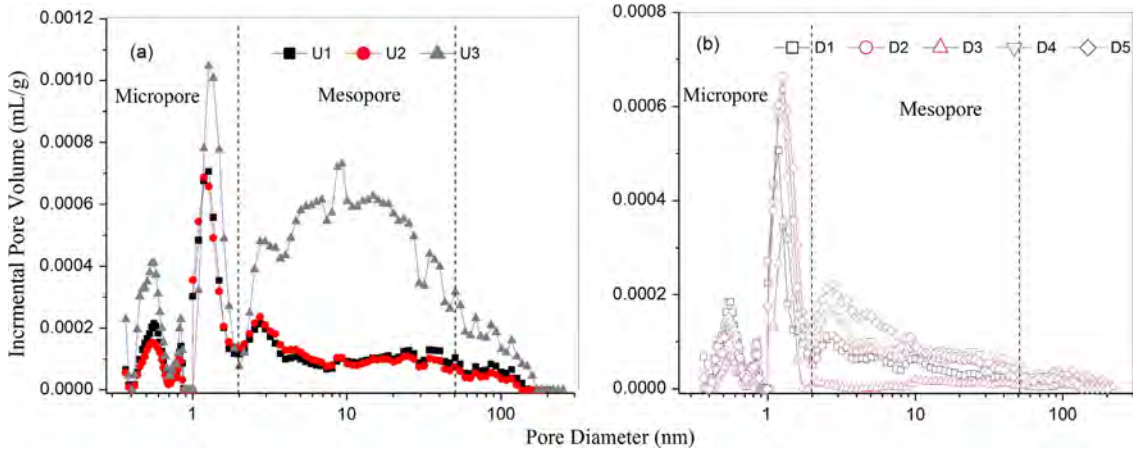

Fig. 4. Pore size distribution defined by incremental pore volume using low pressure gas (LPG) adsorption analyses (N_2 and CO_2). Combined N_2 and CO_2 physisorption at 1 nm using the same calculation model of DFT. Pore diameters range between 0.3 and 200 nm. The boundaries between micro-, meso- and macropores are highlighted by dashed lines.

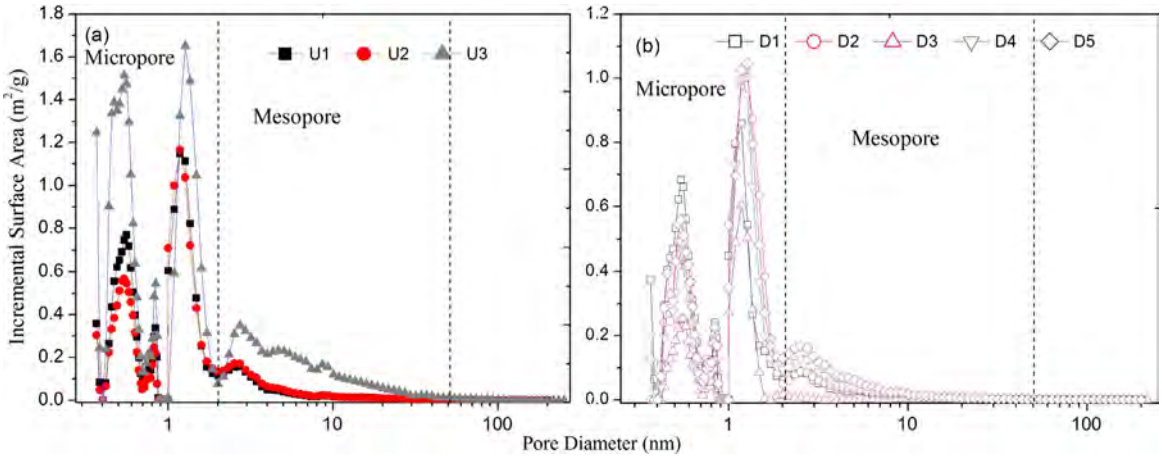

Fig. 5. Pore size distribution defined by incremental surface area using LPG (N_2 and CO_2) analyses. Combined N_2 and CO_2 physisorption at 1 nm using the same calculation model of DFT. Pore diameters range between 0.3 and 200 nm.

is mainly related to the OM and clay mineral contents. The mesopores in clay mineral layer that provide adsorption surface area might disappear due to compression of the tectonic stress. Therefore, the structural deformation can be seen as a negative factor in the nano-pore content, although their clear relationship was still poorly understood.

3.3. Hg porosimetry

The advantages of using the MICP technique are that it directly measures PV through the mercury volume injected, and requires only small rock cuttings or fragments. The total porosity is determined by mercury immersion (bulk density) coupled with helium pycnometry (skeletal density). All nine samples have a similar porosity ranges between 1.3 and 7.5% (Table 2). Although the undeformed shale U3 has the highest porosity and total PV which was determined by MICP, there was no clear correlation between total porosity and total pore volumes for all samples. The PSD by MICP is plotted as incremental pore volume (mL/g; Fig 6) and incremental surface area (m^2/g; Fig 7).The curves from the incremental pore volume versus pore diameter results perfectly reflect PSD (Fig. 6). The PSD parameters derived from the MICP analyses range from 7 to 120,000 nm including the meso- and macropores were shown in (Table 2 and Figs. 6, 7 with the PV and SA). Overall, all samples used in the mercury experiments mainly have a bimodal that pore diameter range from 7 nm to 100 nm and the pore diameter more than 5000 nm (Fig. 6).

The PV generally has a positive relationship with the PSD, whereas there is a negative correlation between the SA and the PSD for a given pore volume [4,15]. All samples show a significant volume of pores with a diameter more than 5000 nm; while these pores do not contribute to the SA of the reservoir as significantly as the finer pores with a diameter range from 7–50 nm (Table 3 and Fig. 7). Undeformed shales have more balance in PV between meso- and macropores, while the deformed shales showed a dominance of macropores (Table 2 and Fig. 6). The results revealed that there was no relationship between structural deformation and total porosity, but the structural deformation had a significant

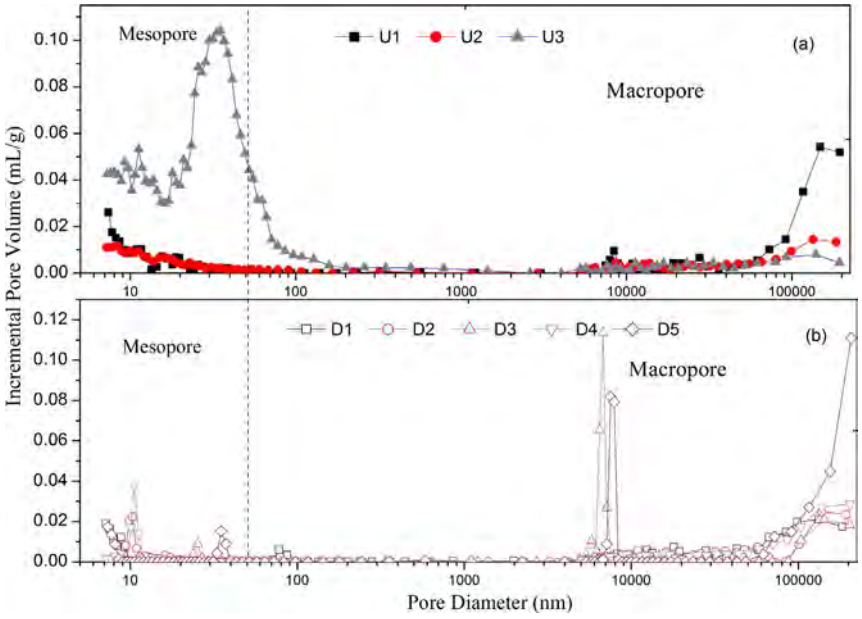

Fig. 6. Pore size distribution defined by incremental pore volume using mercury injection capillary pressure (MICP) analyses. Pore diameters range between 7 nm and 100 μm. The minimum pore diameter is caused by the limitations of the instrument.

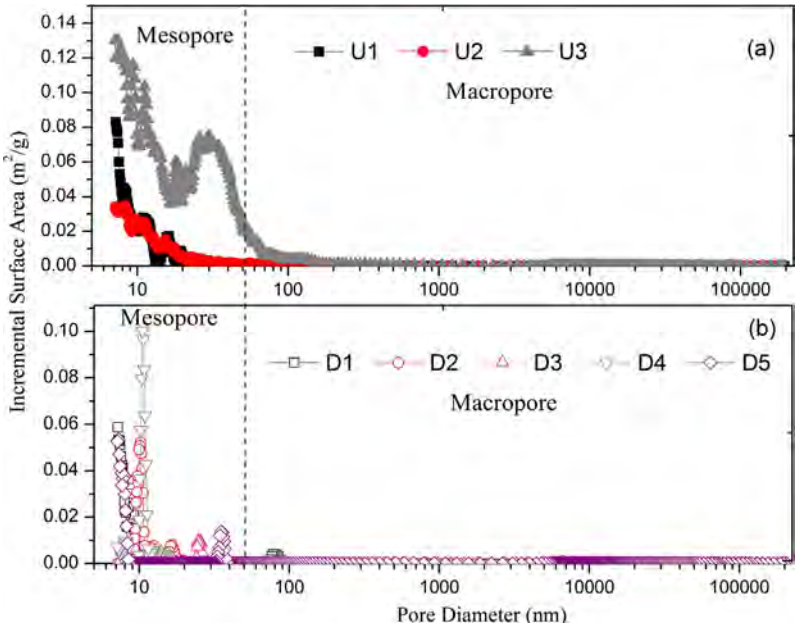

Fig. 7. Pore-size distribution defined by incremental surface area using MICP analyses. Pore diameters range between 7 nm and 100 μm.

effect on the evolution of PSD in shale. Therefore, the structural deformation plays a positive role in the pore size distribution evolution. The structural deformation might convert the mesopores to macropores with connectivity growth, caused by nanoscale cracking.

3.4. Response of pore structure to structural deformation

It is believed that the shale composition controlled the pore structure character, and the diagenetic processes controlled the shale composition [1,14–17]. In the previously analysis, we discussed the pore characteristic data obtained by different analytical methods of MICP and LPG separately. The Fig. 8 shows the correlation between porosity and pore volume for different pore diameters, indicating the positive relationship between porosity and micro- and mesopores PV ($R^2 > 0.85$) for undeformed shale, while the porosity of deformed shale was only related to the macropores PV ($R^2 = 0.77$). Such difference between the deformed and undeformed samples indicated that the micro- and mesopores (nano-scale pores) dominate the total porosity, and controlled by the diagenetic processes and shale compositions in the primary shale reservoir, while the macropores controlled the total porosity in the intense tectonic deformation shale. It is found that there were no significant changes in porosity between deformed and undeformed shale samples. In order to further study the evolution of pore size distribution in deformed shales, analysis method of combined the mercury intrusion and gas adsorption was used to determine the relative content percentage of micro-, meso- and macropores in this article by set the mesopores as a referenced value(Table 2 and Fig 9). The balance of micro-, meso- and macropores were weakened in deformed shale samples, and the percentages of PV in different pore diameters were changed as macropores increased and mesopores decreased.

Organic matter can affect the evolution of pore structure, especially for different organic matter types and organic matter maturity. Jiang et al. reported the pore structure of a lacustrine

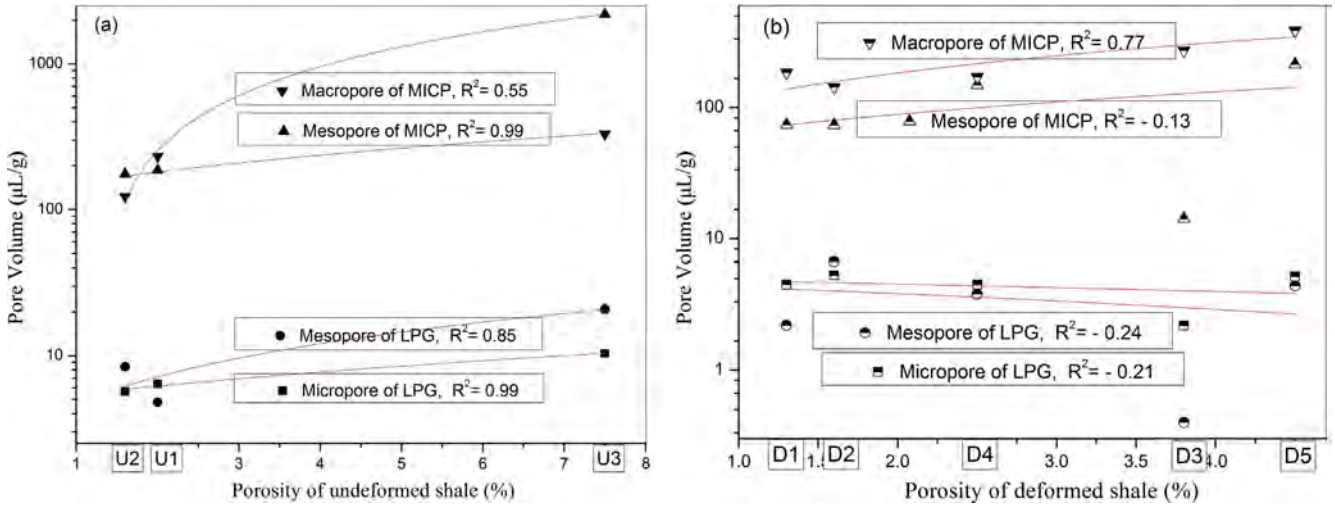

Fig. 8. Relationship between total porosity and pore volume of micro-, meso- and macropores in shale samples from different analytic methods of LPG and MICP.

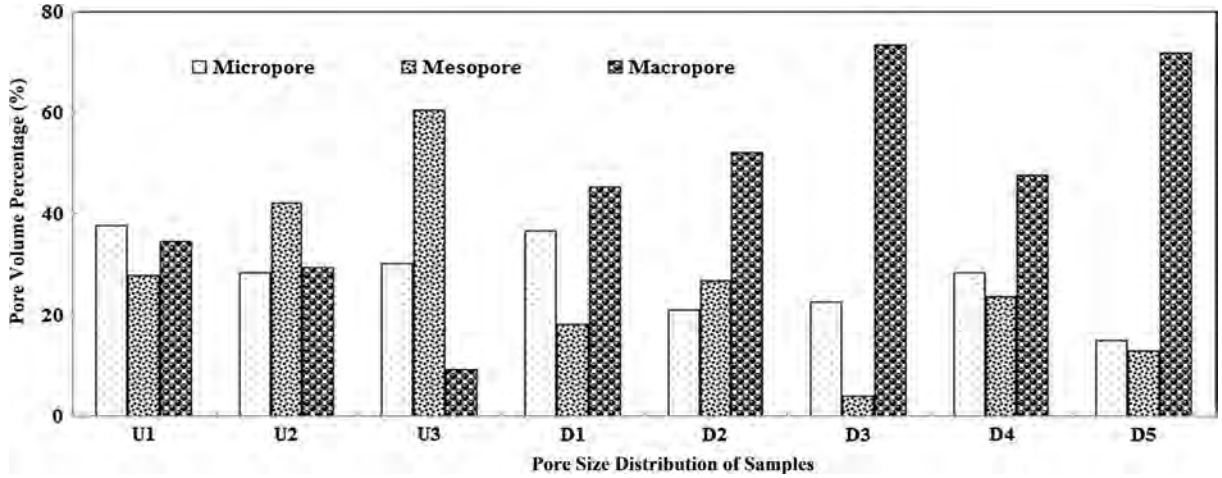

Fig. 9. The pore volume percentages for shale samples.

oil shale in the Ordos Basin, and indicates that the mesopores are dominant in samples [6]. Chen and Xiao measure the evolution of pore structure of artificially matured samples during an anhydrous pyrolysis, finding that the microporosity and mesoporosity increases with thermal maturity after the oil window stage [19]. The effect of organic matter on shale pore structure is mainly concentrated in micropore and mesopore [18–20], and achieve by the difference type and maturity. In present study, all samples have a similar kerogen type and maturity stage, consistent with the similar micropores. Clay minerals can influence pore structure evolution, and always have comparable organic contents. As compared to the deformed shale samples, the undeformed shale samples have higher values in micro-, meso-, total pore SA and adsorption quantity, because they have a higher clay content, rather than because of their undeformation. Ross and Bustin suggested that shales enriched in both clays and organics have the largest micropore volumes, suggesting a micropore contribution from both the organic and clay fractions. In the present study, the shale sample of D3 which poor in clay and TOC has the least micro- and mesopores. Kareem et al. found that the clay minerals are overrepresented at the pore surfaces and in pore spaces compared to the other major mineral as quartz and feldspar [42]. The knowledge of effective mineralogy complicated the influence of clay minerals on the pore structure. The biogenic quartz produced by precipitation during diagenesis with silica derived from graptolite and radiolarians [38], which may also control the pore volume and structure in shales. This type of quartz affects microporosity significantly and has certain correlation to TOC content. There are no clearly-defined relationships between quartz mineralogy and pore structure, because the micropore characteristics of the samples did not change with the quartz content in this study. Furthermore, the parts of extra quartz content in fracture filling of deformed shale may come from the hydrothermal source, after the tectonic deformation and fracture generations. The relationship between shale compositions and pore structure is not well reflected in the change of shale pore structure in deformed shale samples for the present study. There is no significant difference in organic matter content in deformed and undeformed samples, which agrees with a similar microporosity on all of samples. All-scale pore structure analysis reveals that the deformed shale had notable higher macropores percentages than undeformed shale. At the same time, the total porosity and micropores were constant, suggesting that the evolution of pore structure in structural deformed shale was due to part of mesopores was disappeared due to compression of the tectonic stress, and macropores were generated due to the development of microcracks.

4. Conclusions

Due to the multi-tectonic movement, shale reservoirs in China are highly diversified and complicated, which transformed the texture of shale beds and resulted in structure deformed shale with unique pore properties. It is necessary to study how pore structure develops in gas shale influenced by tectonic deformation. In this article, pore structure and its evolution feature investigations were performed using two sets of shale samples (deformed shale and undeformed shale). The shale compositions include minerals and organic matters have a significant influence on the total porosity and pore structure. Gas absorption quantity controlled by the TOC and clay mineral content. With increasing clay content, the N_2 absorption quantity increases significantly. The TOC and clay minerals affected the lower limit of micropore characteristics of shale together. Shale has smaller micropores and mesopores volume when with lower TOC and clay content. While the tectonic deformational could not affect the shale material composition significantly. Tectonic stress and structural deformation have an effect on the pore surface area and adsorption capacity of shale. Undeformed shale has a higher surface area (SA) and N_2 adsorption capacity, and the strong deformed shale samples have the lowest SA and nitrogen adsorption capacity. There were no significant changes in total porosity and pore volume (PV) between deformed shale samples and undeformed shale. However, the structural deformational can affected the evolution of pore size distribution (PSD) by change the material arrangement and improve connectivity of shale. The structural deformation has a significant effect on the evolution of pore size distribution, especially for the increase in the proportion of macroporous. The tectonic deformation also has a slightly effect on the maturity of shale. The deformed shale has a higher VRo than undeformed shale. All of these results provide evidence to the evolution of pore structures of shale affected by tectonically deformation in South China.

Acknowledgments

Analytical assistance with the MICP and LGP was provided by Engineer Tao Zhang. This work was financially supported by the Major State Research Development Program of China (Grant No. 2016YFC0600202) and the China Geological Survey (CGS, Grant No. DD20160183). We thank Dr. Zuohua Huang and anonymous reviewers for their constructive comments that greatly improved this paper.

References

[1] Clarkson CR, Haghshenas B, Ghanizadeh A, et al. Nanopores to megafractures: Current challenges and methods for shale gas reservoir and hydraulic fracture characterization. J Nat Gas Sci Eng 2016;31:612–57.
[2] Ross DJK, Bustin RM. Shale gas potential of the Lower Jurassic Gordondale member, Northeastern British Columbia, Canada. Bull Can Pet Geol 2007;55:51–75.
[3] Chalmers GRL, Bustin RM. The organic matter distribution and methane capacity of the Lower Cretaceous strata of Northeastern British Columbia, Canada. Int J Coal Geol 2007;70:223–39.
[4] Chalmers GRL, Bustin RM, Power IM. Characterization of gas shale pore systems by porosimetry, pycnometry, surface area, and field emission scanning electron microscopy/transmission electron microscopy image analyses: examples from the Barnett, Woodford, Haynesville, Marcellus, and Doig units. AAPG Bull 2012;96(6):1099–119.
[5] Guo TL. Discovery and characteristics of the Fuling shale gas field and its enlightenment and thinking. Earth Sci Frontiers 2016;23:29–43.
[6] Jiang FJ, Chen D, Wang ZF, et al. Pore characteristic analysis of a lacustrine shale: a case study in the Ordos Basin, NW China. Mar Pet Geol 2016;73:554–71.
[7] Ross DJK, Bustin RM. Characterizing the shale gas resource potential of Devonian-Mississippian strata in the Western Canada sedimentary basin: application of an integrated formation evaluation. AAPG Bull 2008;92:87–125.
[8] Loucks RG, Reed RM, Ruppel SC, et al. Morphology, genesis, and distribution of nanometer-scale pores in siliceous mudstones of the Mississippian Barnett Shale. J Sediment Res 2009;79:848–61.
[9] Loucks RG, Reed RM, Ruppel SC, et al. Spectrum of pore types and networks in mudrocks and a descriptive classification for matrix-related mudrock pores. AAPG Bull 2012;96:1071–98.
[10] Sing KSW, Everett DH, Haul RAW, et al. Reporting physisorption data for gas/solid systems with special reference to the determination of surface area and porosity. Pure Appl Chem 1985;57:603–19.
[11] Thommes M, Kaneko K, Neimark AV, et al. Physisorption of gases, with special reference to the evaluation of surface area and pore size distribution (IUPAC Technical Report). Pure Appl Chem 2015;87:1051–69.
[12] Tiwari P, Deo M, Lin CL, et al. Characterization of oil shale pore structure before and after pyrolysis by using X-ray micro CT. Fuel 2013;107:547–54.
[13] Ruppert LF, Sakurovs R, Blach TP, et al. A USANS /SANS study of the accessibility of pores in the Barnett Shale to methane and water. Energ Fuel 2013;27:772–9.
[14] Ross DJK, Bustin RM. The importance of shale composition and pore structure upon gas storage potential of shale gas reservoirs. Mar Pet Geol 2009;26:916–27.
[15] Chalmers GRL, Bustin RM. Lower Cretaceous gas shales in Northeastern British Columbia, Part I: geological controls on methane sorption capacity. Bull Can Pet Geol 2008;56:1–21.
[16] Chalmers GRL, Ross DJK, Bustin RM. Geological controls on matrix permeability of Devonian Gas Shales in the Horn River and Liard basins, northeastern British Columbia, Canada. Int J Coal Geol 2012;103:120–31.
[17] Chalmers GRL, Bustin RM, Bustin AAM. Geological controls on matrix permeability of the Doig-Montney hybrid shale-gas–tight-gas reservoir, northeastern British Columbia (NTS 093P). In: Geoscience BC Summary of Activities 2011, Geoscience BC, Report 2012–1, p. 87–96.
[18] Curtis ME, Cardott BJ, Sondergeld CH, et al. Development of organic porosity in the Woodford Shale with increasing thermal maturity. Int J Coal Geol 2012;103:26–31.
[19] Chen J, Xiao X. Evolution of nanoporosity in organic-rich shales during thermal maturation. Fuel 2014;129:173–81.
[20] Sun LN, Tuo JC, Zhang MF, et al. Formation and development of the pore structure in Chang 7 member oil-shale from Ordos Basin during organic matter evolution induced by hydrous pyrolysis. Fuel 2015;158:549–57.
[21] Liu SG, Deng B, Zhong Y, et al. Unique geological features of burial and superimposition of the Lower Paleozoic shale gas across the Sichuan Basin and its periphery. Earth Sci Frontiers 2016;23:11–28.
[22] Guo TL, Zeng P. The structural and preservation conditions for shale gas enrichment and high productivity in the Wufeng-Longmaxi Formation, Southeastern Sichuan Basin. Energy Explor Exploit 2015;33:259–76.
[23] Ma Y, Zhong NN, Han H, et al. Definition and structure characteristics of pores in mylonitized organic-rich shales. Sci China: Earth Sci. 2014;2014 (44):2202–9.
[24] Wang ZX, Zhang J, Guan HM, et al. A discussion on the structural deformation and oil/gas traps on the western side of the Xuefeng Mountain. Geol Bull China 2012;31:1812–25.
[25] Ibanez WD, Kronenberg AK. Experimental deformation of shale: Mechanical properties and micromechanical indicators of mechanisms. Int J Rock Mech Min 1993;30:723–34.
[26] Pan JN, Hou QL, Ju YW, et al. Coalbed methane sorption related to coal deformation structures at different temperatures and pressures. Fuel 2012;102:760–5.
[27] Pan JN, Zhu HT, Hou QL, et al. Macromolecular and pore structures of Chinese tectonically deformed coal studied by atomic force microscopy. Fuel 2015;139:94–101.
[28] Xie Y, Wang J, Wang ZJ, et al. Advance of comprehensive hydrocarbon geological survey and research of Sinian-Lower Paleozoic within the mountain-Basin transition zone of west side of Xuefeng Mountains, in Middle-Upper Yangtze region of Southern China. Geol Bull China 2012;31:1750–68.
[29] Washburn EW. The dynamics of capillary flow. Phys Rev 1921;17:273–83.
[30] Thommes M, Cychosz KA. Physical adsorption characterization of nanoporous materials: progress and challenges. Adsorption 2014;20:233–50.
[31] Landers J, Gor AGA, Neimark V. Density functional theory methods for characterization of porous materials. ChemInform 2014;437:3–32.
[32] Groen JC, Peffer LAA, Perez-Ramírez J. Pore size determination in modified micro- and mesoporous materials. Pitfalls and limitations in gas adsorption data analysis. Microporous Mesoporous Mater 2003;60:1–17.
[33] Jarvie DM, Hill RJ, Rurle TE, et al. Unconventional shale-gas systems: the Mississippian Barnett shale of north-central texas as one model for thermogenic shale-gas assessment. AAPG Bull 2007;91:475–99.
[34] Liu WH, Xu YC, Zhang SC, et al. A new kind of mechanism for hydrocarbon generated-mechanochemistral function and experimental prove. Acta Sedimentol Sin 2000;18:314–8.
[35] Popp BN, Parekh P, Tilbrook B, et al. Organic carbon d13C variations in sedimentary rocks as chemostratigraphic and paleoenvironmental tools. Palaeogeogr Palaeoclim Palaeoecolo 1997;132:119–32.
[36] Dawson TE, Mambelli S, Plamboeck AU, et al. Stable isotopes in plant ecology. Ann Rev Eco Syst 2002;33:507–59.
[37] Lewan MD. Stable carbon isotopes of amorphous kerogens from Phanerozoic sedimentary-rocks. Geochim Cosmochim Acta 1986;50:1583–91.
[38] Luo QY, Zhong NN, Dai N, et al. Graptolite-derived organic matter in the Wufeng-Longmaxi Formations (Upper Ordovician-Lower Silurian) of southeastern Chongqing, China: Implications for gas shale evaluation. Int J Coal Geol 2016;153:87–98.
[39] Wortman JJ, Evans RA. Young's modulus, shear modulus Poisson's ratio in silicon and germanium. J Appl Phys 1965;36:153–6.
[40] Ding WL, Li C, Li CY, et al. Fracture development in shale and its relationship to gas accumulation. Earth Sci Front 2012;19:212–20.
[41] Zhang XB, Wang ZX, Cao ZY. Experimental study on the relationship between brittle deformation, fracturing and gas adsorption capacity. In: Presented at the Project Annual Conference held in Beijing, 2016, 9–10 December.
[42] Kareem R, Cubillas P, Gluyas J, et al. Multi-technique approach to the petrophysical characterization of berea sandstone core plugs (Cleveland Quarries, USA). J Petrol Sci Eng 2017;149:436–55.